European Journal of Orthodontics, 2021, 708–717
https://doi.org/10.1093/ejo/cjab065
Advance Access publication 3 September 2021

Original article

Bone remodelling patterns around orthodontic mini-implants migrating in bone: an experimental study in rat vertebrae

Kathrin Becker[1,*], Nicole Rauch[2,*], Giulia Brunello[2,3], Sarah Azimi[1], Mathias Beller[4,5], Mira Hüfner[1], Manuel Nienkemper[1,6], Beryl Schwarz-Herzke[7,†] and Dieter Drescher[1,†]

[1]Department of Orthodontics, University Clinic of Düsseldorf, Germany
[2]Department of Oral Surgery, University Clinic of Düsseldorf, Germany
[3]Department of Neurosciences, University of Padua, Italy
[4]Institute for Mathematical Modeling of Biological Systems, University of Düsseldorf, Germany
[5]Systems Biology of Lipid Metabolism, University of Düsseldorf, Germany
[6]Private Practice, Dusseldorf, Germany
[7]Institute for Anatomy II, University Clinic of Düsseldorf, Germany

*Both authors contributed equally.
†Both authors contributed equally.

Correspondence to: Kathrin Becker, Department of Orthodontics, University Clinic of Düsseldorf, Moorenstr. 5, 40225 Düsseldorf, Germany. E-mail: kathrin.becker@med.uni-duesseldorf.de

Summary

Background: Orthodontic implant migration has been clinically observed in presence of continuous loading forces. Recent studies indicate that osteocytes play a crucial role in this phenomenon.
Objectives: Aim of this study was to investigate local osteocytic gene expression, protein expression, and bone micro-structure in peri-implant regions of pressure and tension.
Material and methods: The present work reports a complementary analysis to a previous micro-computed tomography study. Two customized mini-implants were placed in one caudal rat vertebra and connected by a nickel–titanium contraction spring generating different forces (i.e. 0, 0.5, 1.0, and 1.5 N). Either at 2 or 8 weeks, the vertebrae were harvested and utilized for 1. osteocytic gene expression using laser capture micro-dissection on frozen sections coupled with qPCR, 2. haematoxylin–eosin staining for qualitative and quantitative analyses, 3. immunofluorescence staining and analysis, and 4. bone-to-implant contact on undecalcified samples.
Results: At the two time points for all the performed analyses no significant differences were observed with respect to the applied force magnitudes and cell harvesting localization. However, descriptive histological analysis revealed remarkable bone remodelling at 2 weeks of loading. At 8 weeks the implants were osseointegrated and, especially in 1.0 and 1.5 N groups, newly formed bone presented a characteristic load bearing architecture with trabecula oriented in the direction of the loading.
Conclusions: The present study confirmed that stress-induced bone remodelling is the biological mechanism of orthodontic implant migration. Bone apposition was found at 'tension' and 'pressure' sites thus limiting implant migration over time.

Introduction

Clinical observations suggested that orthodontic implants can migrate within the bone when subject to continuous loading (1–5). Recently, a preclinical study in the rat-tail model employing high-resolution *in vivo* micro-computed tomography (micro-CT) revealed an association between applied force magnitude and implant displacement. Additionally, the implant migration velocity within the bone decreased over time (6). Therefore, it is likely that implant migration is accompanied by bone remodelling, which, however, has not yet been verified.

Clinical trials are not eligible to assess the underlying molecular patterns of implant migration. In fact, information on bone remodelling is frequently derived from *in vivo* studies (7), which are often limited to end-point analyses (8, 9). Matching *post-mortem* molecular and histological analyses with the longitudinal data from repetitive non-destructive *in vivo* micro-CT can not only overcome this limitation but also provide a deeper understanding of the peri-implant load-driven bone remodelling (10–12).

Analysis of load-driven mechanotransduction has emerged as a fundamental step to elucidate the impact of orthodontic loads on peri-implant tissues (13, 14). Osteocytes are recognized to be the principal sensory cells responding to mechanical stimuli that alter the interstitial fluid flow (12). They have been also demonstrated to propagate the sensed signals to other osteocytes through gap junctions (15). In reaction to the mechanical stimuli, the expression of sclerostin by osteocytes is downregulated, leading to an activation of the Wnt signalling pathway, which favours bone formation (16). Moreover, when a load of sufficient magnitude is applied to the bone, as in case of orthodontic implants, microcracks can affect the integrity of the canalicular network. As a consequence, dendritic processes are more likely to be interrupted, inducing osteocyte apoptosis, which has been shown to trigger osteoclast formation and thus bone resorption (17).

In recent years, harvesting of single cells from undecalcified cryosections was achieved utilizing an advanced technology termed laser capture micro-dissection (LCM) (18). It allows analysis of gene expression in osteocyte subpopulations, which are directly or indirectly affected by the mechanical stimuli from migrating implants. Based on time-lapsed *in vivo* micro-CT observations documenting implant migration direction, it is possible to selectively collect cells from areas subjected to different load qualities (12).

Previously, we investigated orthodontic implant migration using micro-CT (6). The data suggested that bone resorption took place mainly in areas at which pressure was suspected to occur, whereas newly formed bone was observed at the initial implant positions. At the end-point, the non-destructive method allowed the authors to utilize the retrieved samples for further molecular and histological examinations.

To elucidate the puzzling phenomenon of orthodontic implant migration, the present manuscript aimed to analyse osteocytes' load-dependent gene expression in cortical areas of compression and tension, as computed from previous longitudinal micro-CT data. The secondary aim consisted in investigating peri-implant bone microstructure and composition, as well as the production of proteins involved in bone remodelling.

Materials and methods

Animals and study design

The protocol has been described in detail previously (6) and was approved by the appropriate local authority (Landesamt für Natur und Verbraucherschutz), Ref. no. 84-02.04.2016.A380, and conformed with the Animal Research: Reporting of In Vivo Experiments (ARRIVE) Guidelines (19). Briefly, two customized Ti–6Al–4V mini-implants, 0.8 in diameter and 3.0 mm in length (RISystem AG, Landquart, Switzerland), were inserted into the dorsal portion of a single tail vertebra in n = 61 female Wistar rats (age 15.4 ± 3.9 weeks). The implants were connected with a nickel–titanium (Ni–Ti) contraction spring operating in the elastic range and randomly assigned to one of the following loading forces: 0 N (control), 0.5, 1.0, and 1.5 N. Half of the animals were sacrificed at 2 weeks and the remaining at 8 weeks after surgery. For the present investigation, a total of 54 animals were available. Vertebrae were retrieved immediately after the sacrifice and subjected to different analyses, as presented in Figure 1.

Peri-implant regions of interest

Assessment of the local stresses and strains occurring around implants is complex. To analyse the patterns of biological response in the peri-implant regions, it was decided to subdivide the peri-implant region into different sectors as detailed below. According to the previous micro-CT analyses, implants were tipping in the directions of load. Therefore, the traditional terminology from orthodontic tooth movements was adopted, defining the 'lateral top' and 'medial bottom' as 'tension' zones and the 'medial top' and 'lateral bottom' regions as zones of 'pressure'. The authors are aware that this is a simplification and that no conventional 'tension' is possible due to the absence of a periodontal ligament. The terminology was chosen because orthodontists are familiar with this concept.

Gene-expression analysis

Sample preparation

After careful preparation of the vertebra and removal of the implants, the samples were embedded in an optimal cutting temperature medium (NEG-50™, Thermo Fisher Scientific Inc., Waltham, Massachusetts, USA). To conserve the vertebra's three-dimensional orientation, the upper right corner of each sample was marked, before freezing the samples at –80°C.

The samples were cut using a cryotome (Leica CM3050 S, Leica Mikrosysteme Vertrieb GmbH, Wetzlar, Germany) equipped with blades for undecalcified tissues (MX35 Premier, Thermo Fisher Scientific Inc.), to obtain slices of 3-µm thickness orthogonally to the longitudinal axis of the implants, as described in Figure 2. The temperature within the cryotome chamber was set at –25°C. A special cryofilm was placed onto the samples' longitudinal surface

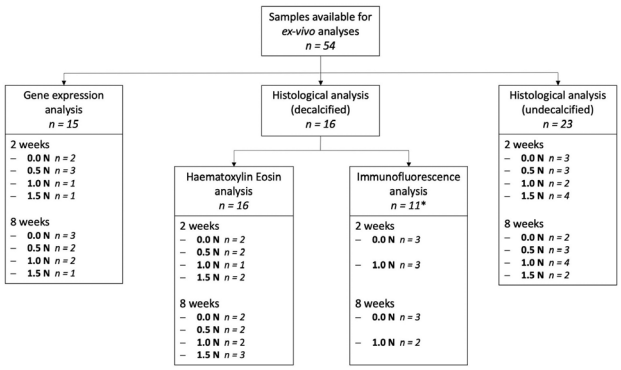

Figure 1. Flowchart of the performed analyses, indicating the number of samples used for each evaluation. *In total, 11/16 samples eligible for automated analysis.

according to Kawamoto and Kawamoto (18) (LMD film type 2, SECTION-LAB Co. Ltd, Hiroshima, Japan), for preserving the sample integrity during the process of cryo-sectioning. The obtained slices were positioned onto glass slides (Starfrost®, Waldemar Knittel Glasbearbeitungs GmbH, Braunschweig, Germany) and stained with Cresyl violet after descending alcohol series (i.e. 100, 90, and 75 per cent).

Laser capture micro-dissection

Up to a distance of 100 µm from each implant site, single osteocytes were extracted from the slices using a LCM technique (PALM MicroBeam, Carl Zeiss AG, Oberkochen, Germany). Osteocyte collection was performed from the cortical bone around each implant, on the 'pressure' (medial top) and 'tension' (distal top) separately (Figure 2). Osteocytes were collected within adhesive caps (AdhesiveCap opaque 500 µl, Carl Zeiss AG) and stored at −80°C until further processing.

Gene-expression analysis

Following the collection of osteocytes, total messenger RNA (mRNA) was extracted using the micro RNeasy kit (Qiagen, Hilden, Germany) as recommended by the manufacturer. Equal amounts of the extracted mRNA were converted to complementary DNA using the QuantiTect Reverse transcription kit (Qiagen). For reverse transcription, random Hexamers and poly T primers were used following the manufacturer's recommendations. Quantitative analyses were performed with a subsequent polymerase chain reaction (PCR) program (Applied Biosystems StepOne™ Real-Time PCR Systems, Thermo Fisher Scientific Inc.) according to the following parameters: 30 seconds denaturation at 95°C and 30 seconds annealing at 60°C. This cycle was repeated 40 times. The amplification was performed using SYBR green reagents (KAPA SYBR® FAST quantitative PCR (qPCR) Kit master mix ABI Prism®, KAPA Biosystems, Cape Town, South Africa) and primers. The list of utilized primers and related sequences are presented in Table 1. H1-0 was used as housekeeping gene. Based on the average of the Ct values of the housekeeping gene, the relative expression levels of RUNX2, SP7, SOST, and CTSK were calculated (20).

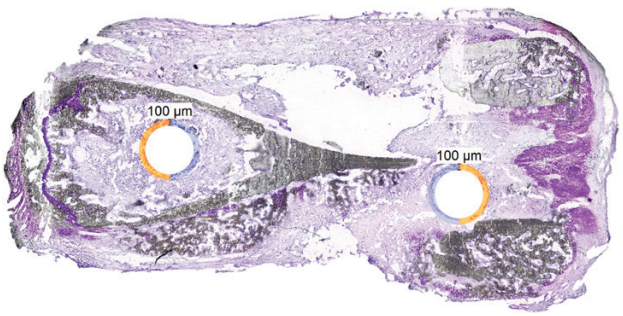

Figure 2. Representative undecalcified fresh frozen sample stained with Cresyl violet showing the cortical bone areas (medial: violet, lateral: orange) for the collection of single cells, i.e. osteocytes, using laser capture microdissection (LCM).

Histological analysis of decalcified samples

Specimen preparation and paraffin-sectioning

After careful preparation of the vertebra and removal of the mini-implants, the samples were stored in 4 per cent formalin (LaboChem, neoLab Migge GmbH, Heidelberg, Germany). Subsequently, bone tissue was decalcified within a custom-made solution of Tris(hydroxymethyl)aminomethane (Merck KGaA, Darmstadt, Germany) dissolved in distilled water and containing ethylenenitrinoltetraacetic disodium-dihydrate (Tritriplex® III, Merck KGaA) for 3 weeks. The solution was changed once a week. After the samples were decalcified, each specimen was divided along its longitudinal axis, so that both implant sites were exposed to the surface, and each half embedded in paraffin. The samples were then cut in a microtome (PFM Medical Slide 4004M, PFM Medical AG, Cologne, Germany) with special blades (MX35 Premier, Thermo Fisher Scientific Inc.) at a thickness of 3 µm and placed onto special sample slides (TOMO® Adhesion Microscope Slides, Matsunami Glass USA Inc., Bellingham, Washington, USA) for either haematoxylin and eosin (HE) staining or immunofluorescence analysis.

Haematoxylin eosin staining and analysis

For the staining process the samples needed to be deparaffinized with xylene and rehydrated by using a descending alcohol series (100, 95, and 90 per cent). The samples were washed with distilled water and stained with HE. Then, the samples were dehydrated using an ascending alcohol series (90, 95, and 100 per cent), rinsed with xylene, covered with a glass coverslip, and scanned with a camera (Basler AG, Ahrensburg, Germany) mounted on a microscope (Olympus BX 51, Olympus Europa SE & Co. KG, Hamburg, Germany) at a magnification of ×20.

Histomorphometric analyses were performed with ImageJ (FIJI distribution) (21). A grid (100 × 100 µm^2) was positioned, and the number of empty lacunae (i.e. not occupied by osteocytes) per total lacunae (EL/TL) was counted manually at a distance of 200 µm from the implant surface.

For the analysis of the bone area per tissue area (BA/TA), a grid (120 × 120 µm^2) was used, and each box up to at a distance of 120 µm from the implant surface was classified as 'bone' if more than 50 per cent of its area was occupied by bone.

Immunofluorescence staining and analysis

For immunofluorescence staining, paraffin was removed using the following ingredients for dewaxing: ROTI®-Histol (Carl Roth GmbH + Co. KG, Karlsruhe, Germany) and an 18:1:1 alcohol mixture of ethanol (100 per cent), methanol (100 per cent), and isopropanol (100 per cent). Slides were washed in a subsequent series of ROTI®-Histol for 10 minutes twice, following a descending

Table 1. Summary of utilized primers.

Gene symbol	Forward primer (5′ → 3′)	Reverse primer (5′ → 3′)	Product length (bp)	Encoding protein
H1-0	CCAAGAGAAGGAAGAACCGCA	GTAGATGCGCGCCAGAGAC	113	Histone H1.0
RUNX2	ACAAATCCTCCCCAAGTGGC	GGATGAGGAATGCGCCCTAA	152	Runx2
SP7	TTTCTGCGGCAAGAGGTTCA	TTGCTCAAGTGGTCGCTTCT	126	Osterix
SOST	AGTCGAGTTCAAGTGGGCTG	TGTTCCATAGCCTCCTCCGA	156	Sclerostin
CTSK	TACCCATATGTGGGCCAGGA	TTCAGGGCTTTCTCGTTCCC	107	Cathepsin K

alcohol series (100, 95, and 80 per cent). Slides were rinsed with distilled water.

Prior to an incubation at 37°C for 1 hour, slides were prepared with a blocking buffer [5 per cent of goat serum, 1 per cent bovine serum albumin, 0.1 per cent Triton X-100, 0.05 per cent Tween 20, everything diluted in 1× phosphate-buffered saline (PBS)]. Subsequently, the slides were incubated with the primary antibodies for osteocalcin (Human/Rat Osteocalcin Antibody, Monoclonal Mouse IgG, R&D Systems Inc., Minneapolis, Minnesota, USA) and cathepsin K (Anti-Cathepsin K, Polyclonal Rabbit IgG, Abgent Inc., California, USA) and incubated at 37°C for 1 hour. Afterwards, the samples were rinsed in 1× PBS for 5 minutes twice. For secondary antibodies (goat anti-Mouse for osteocalcin, Alexa Fluor® Plus 488, and goat anti-Rabbit for cathepsin K, Alexa Fluor® Plus 568, Thermo Fisher Scientific Inc.), the samples were incubated at 37°C for 30 minutes, and after that rinsed in 1× PBS for 5 minutes twice. For the staining of the nuclei, 4′,6-diamidino-2-phenylindole (DAPI) was used (DAPI solution, Thermo Fisher Scientific Inc.). After incubation, a mounting medium (Fluoromount-G®, Southern Biotech Inc., Birmingham, Alabama, USA) was applied prior to the coverslip onto the sample front.

The whole slides were then scanned at a magnification of ×40 using a fluorescence microscope (Operetta CLS™ high-content analysis system, PerkinElmer Inc., Waltham, Massachusetts, USA).

In order to assess the amount of expressed osteocalcin and cathepsin K, images were analysed with ImageJ (FIJI distribution). Four regions of interest (ROIs) were defined by subdividing the peri-implant region (up to a distance of 500 µm to the former implant) into 'tension' zones (i.e. 'lateral top' and 'medial bottom') and 'pressure' zones (i.e. 'lateral bottom' and 'medial top'; Figure 3). In each ROI, the amount of osteocalcin and cathepsin K and the number of nuclei were calculated using an open-source software (CellProfiler®, BSD 3-clause, Broad Institute of MIT and Harvard, USA). For each signal, the quotient of the occupied area per tissue area was extracted.

Histological analysis of undecalcified samples

Specimen preparation

The samples were fixated in formalin 4 per cent (LaboChem, neo-Lab Migge GmbH). They were dehydrated using ascending grades of alcohol (70, 80, 90, 96, and 99 per cent) and xylene, infiltrated and embedded in methylmethacrylate (Technovit® 9100; Kulzer GmbH, Wehrheim, Germany) for non-decalcified sectioning. During this standardized procedure, any negative influence of polymerization heat was avoided due to a controlled polymerization in a cold atmosphere (4°C). After 20 hours, the sample were completely polymerized. Each vertebra was cut orthogonal to the long axis of the two parallel implants using a band saw (Exakt®; Apparatebau, Norderstedt, Germany); 300 µm in thickness were prepared, glued with acrylic cement (Technovit® 7210 VLC; Kulzer GmbH) to silanized glass slides (Super Frost; Menzel GmbH, Braunschweig, Germany), and ground to a final thickness of approximately 70 µm. Subsequently, all specimens were stained with toluidine blue.

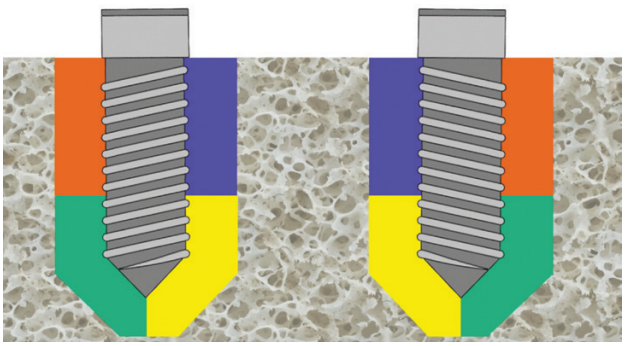

Figure 3. Graphical representation of the regions of interest of 'pressure', i.e. 'lateral bottom' (green), 'medial top' (violet) and of 'tension', i.e. 'lateral top' (orange) and 'medial bottom' (yellow).

Bone-to-implant contact

The whole slides were digitized using a camera (Basler) mounted on a microscope (Olympus BX 51) at a magnification of ×20. The relative amount of calcified tissue in direct contact with the implants, i.e. the bone-to-implant contact (BIC), was quantified using ImageJ and expressed as percentage (per cent).

Statistical analysis

The statistical analysis was performed using the open-source software program R (22). For descriptive purposes, boxplots were created. The R package *lme4* (23) was used to perform a linear mixed effects analysis of the relationship between the respective outcome variables and applied force, and localization ('tension'/'pressure' zone). As fixed effects, we entered the applied force (0, 0.5, 1.0, and 1.5 N) and the localization. As random effects, we had intercepts for animals. Visual inspection of residual plots did not reveal any obvious deviations from homoscedasticity or normality. *P*-values were obtained by likelihood ratio tests of the full model with the effect in question against the model without the effect in question. The results were found significant at $P < 0.05$.

Results

Gene-expression analysis

Osteocytes were harvested by single cell LCM from two cortical regions around the implants to investigate expression of genes involved in bone remodelling in the cortical compartment at two time points (2 and 8 weeks), and particularly relevant for bone formation (Runx2, osterix) and resorption (sclerostin, cathepsin K). The main results are presented in Supplementary Figures S1–S4, showing data retrieved from the medial areas of 'pressure' in violet and in orange bars data from the lateral 'tension' areas. At both time points, for all the investigated genes, no significant differences were found for the effects localization (i.e. 'tension' and 'pressure') and force (i.e. 0.0, 0.5, 1.0, and 1.5 N).

Runx2

At two weeks, there was a tendency of higher expression of Runx2 on the 'tension' site of the implants in the 1.5 N group, while the opposite was observed in the 0.5 and 1.0 N groups. At 8 weeks, expression of Runx2 was by trend higher at the 'pressure' sites in all test groups, and the difference was greater the higher the applied force was.

Osterix

At two weeks, there was a trend towards a higher relative expression of osterix at the lateral 'tension' site compared to the medial 'pressure' zone in all groups except the 1.0 N group. At 8 weeks of loading, the opposite trend was observed in three groups out of four. Additionally, at both time points, the 0.5 N group reached the highest values.

Sclerostin

At 2 weeks, at the 'tension' and 'pressure' sites the expression of Sclerostin decreased with increasing force magnitude in the three test groups. At 8 weeks of loading, the relative expression was by trend higher at the medial 'pressure' site in 0.5 and 1.0 N groups and increased in the 'tension' sites with increasing force magnitude in the test groups. There was also a tendency of overexpression at the lateral 'tension' compared to the medial 'pressure' site in the 1.5 N group where Sclerostin values.

Cathepsin K

At both time points, lateral 'tension' site values were by trend lower to the medial 'pressure' sites, except in the 1.5 N group at 2 weeks.

Decalcified histology and histomorphometry

Histological analysis

Histological HE stained sections from different loading groups at 2 and 8 weeks are presented in Figure 4a–4d and 4e–4h, respectively. After 2 weeks of loading, bone formation and presence of mesenchymal stem cells and osteoclasts were observed mainly in the cancellous compartment. The presence of osteoid matrix combined with osteoclastic resorption lacunae testified the ongoing bone remodelling around the implants. In the highest loading group (Figure 4d), the cortical compartment presented a denser and thicker woven bone layer on both 'pressure' and 'tension' sites. Whereas osteoclastic resorption seemed to be more pronounced in the 'pressure' zones, no differences in bone formation were observed among the groups.

At 8 weeks a maturation and mineralization of peri-implant bone were observed in all samples, with no evident boundary between pristine and newly formed bone. Fibrous tissue could not be observed along implant contours. Interestingly, in the distal peri-implant cortical compartment ('tension' site) of the sample subject to the highest load, bone remodelling and presence of osteoclasts and mesenchymal stem cells were still observed (Figure 4h). When a high force was applied (1.0 and 1.5 N), the thickening of the trabeculae was observed on the compression 'medial top' areas, suggesting an enhanced bone formation activity associated with a higher mechanical strain (Figure 4d). Interestingly, trabecular orientation seemed to be influenced by the compression force. Additionally, thickening of bone apposition and thickening of the cortical compartment were observed and were most pronounced in the 1.5 N group.

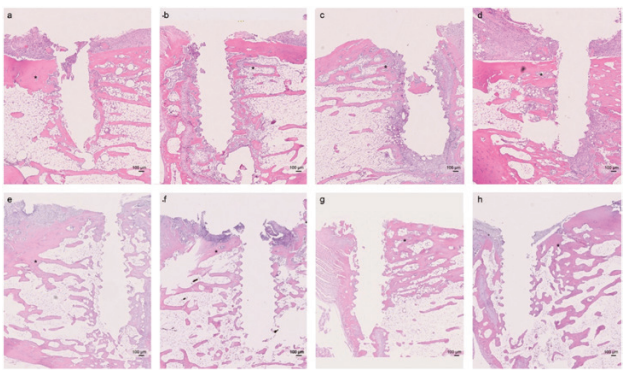

Figure 4. Representative histologic samples [haematoxylin and eosin (HE)] after two weeks (a–d) and 8 weeks (e–h) of loading with 0.0 N (a, e), 0.5 N (b, f), 1.0 N (c, g), and 1.5 N (d, h). The 'medial top' compression area is identified with an asterisk (*).

Histomorphometric analyses

For histomorphometric analyses, data from peri-implant 'medial top' and 'lateral bottom' 'pressure' sites and 'lateral top' and 'medial bottom' 'tension' sites were assessed at both time points. At both time points, for both EL/TL and BA/TA, no significant differences were found for the effects localization (i.e. 'tension' and 'pressure') and force (i.e. 0.0, 0.5, 1.0, and 1.5 N).

Occupied lacunae

At 2 and 8 weeks of loading, the control group (0 N) exhibited a similar ratio of EL/TL on both sites. At 2 weeks in 0.5 and 1.0 N groups higher values were found on the pressure sites, whereas the opposite was observed in the 1.5 N group (Figure 5). At 8 weeks in all three test groups higher EL/TL values were recorded on the 'pressure' sites as compared to the 'tension' sites. Regardless of the site, these values tended to increase with increasing applied force.

BA/TA

At 2 weeks similar values were registered on 'pressure' and 'tension' sites. However, in all groups except one (1.5 N) the BA/TA was slightly higher in the compression areas (Figure 6). At 8 weeks, this

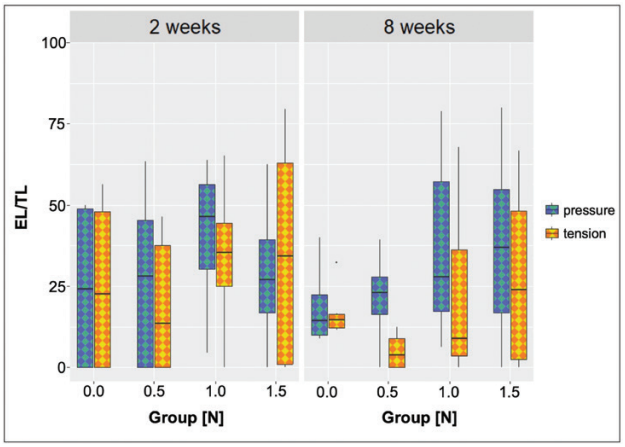

Figure 5. Analysis of empty lacunae per total lacunae (EL/TL) at 2 and 8 weeks in the 'medial top' and 'lateral bottom' 'pressure' sites of the implants (in violet and green) and in the 'lateral top' and 'medial bottom' 'tension' ones (in orange and yellow).

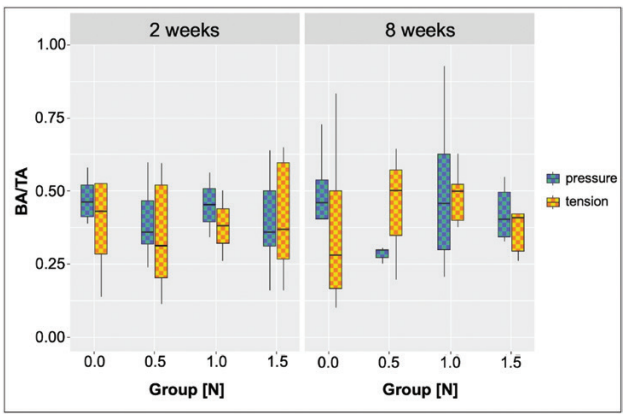

Figure 6. Analysis of the bone area per tissue area (BA/TA) at 2 and 8 weeks in the 'medial top' and 'lateral bottom' 'pressure' sites of the implants (in violet and green) and in the 'lateral top' and 'medial bottom' 'tension' ones (in orange and yellow).

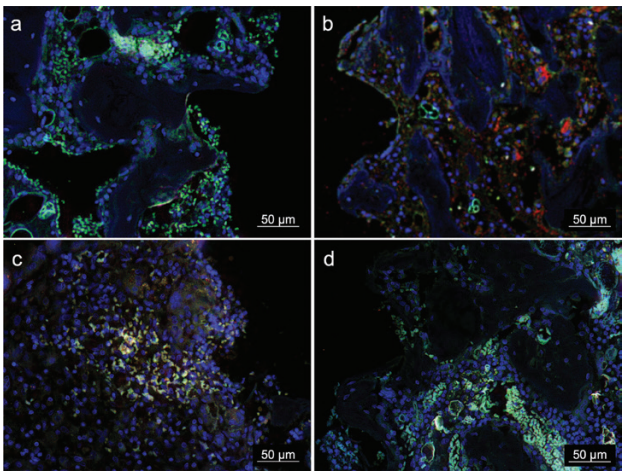

Figure 7. Representative immunofluorescence images after 2 weeks of loading (1.0 N) showing the expressions of osteocalcin (in green) and cathepsin K (in red) in the following regions of interest: (a) lateral top, (b) medial top, (c) lateral bottom, and (d) medial bottom. Nuclei shown by DAPI staining (in blue).

tendency was maintained in the control, while in the 0.5 and 1.0 N groups lower values were observed in the 'pressure' sites.

Immunofluorescence analysis

Fluorescence imaging was applied to investigate the distribution of two proteins involved in bone remodelling at two time points (i.e. 2 and 8 weeks) in peri-implant areas of 'pressure' and 'tension'. Overall, both osteocalcin and cathepsin K were highly expressed in the early phase of healing (Figure 7), while their levels were dramatically reduced after 8 weeks regardless of the loading. At 2 and 8 weeks of loading, for both osteocalcin and cathepsin K, no statistical differences were observed for the factors localization and group (Figure 8a and 8b).

Osteocalcin

At 2 weeks, in the group subject to load (1.0 N) the expression of osteocalcin was higher by trend in the 'tension' sites, as compared to the 'pressure' ones. This is also visible in Figure 7, where the green signal for the expression of osteocalcin was detected to a higher extend in the 'tension', i.e. 'lateral top' and 'medial bottom' (Figure 7a and 7d) sites than in the 'pressure' sites (Figure 7b and 7c). By contrast, in both loading groups osteocalcin was detectable to a lower extend at 8 weeks as compared to 2 weeks.

Cathepsin K

Cathepsin K, which is an important marker to identify bone resorption, was present in both groups at 2 weeks, while it was hardly detectable in the late phases of healing in the test as well as in the control group.

Undecalcified histology and bone-to-implant contact

Histological analysis

To investigate the osseointegration of the implants, undecalcified histology was performed, demonstrating the bone architecture along the implants. At 8 weeks, they were found to be osseointegrated, with close apposition of newly formed bone up to the neck of the implants, as revealed by toluidine blue staining the older bone as violet blue and the newly formed bone as intense blue (Figure 9a). At higher magnification, the bone facing the implant surface still presented areas of woven bone and layers of lamellar bone at 8 weeks, indicating a recent and persisting high bone remodelling (Figure 9b).

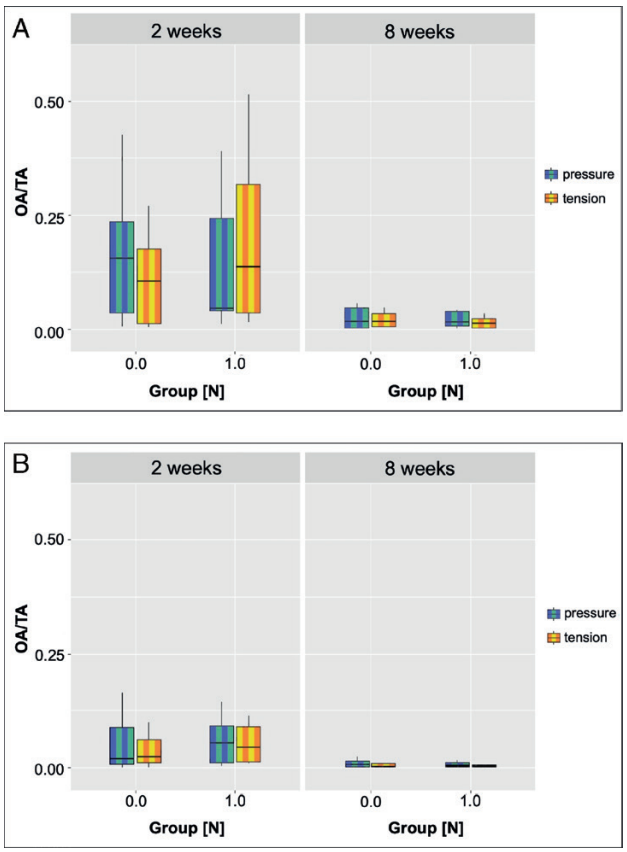

Figure 8. (a) Expression of osteocalcin at 2 and 8 weeks in the 'medial top' and 'lateral bottom' 'pressure' sites of the implants (in violet and green) and in the 'lateral top' and 'medial bottom' 'tension' ones (in orange and yellow). (b) Expression of cathepsin K at 2 and 8 weeks in the 'medial top' and 'lateral bottom' 'pressure' sites of the implants (in violet and green) and in the 'lateral top' and 'medial bottom' 'tension' ones (in orange and yellow). OA/TA, occupied area per tissue area.

Bone-to-implant contact

After 2 weeks of loading, the BIC was lower under an applied force (0.5, 1.0, and 1.5 N) compared to the control group (Figure 10). Force resulted to have no significant effect on BIC values after a healing period of 2 weeks. In all test groups, BIC trended to increase overtime, with greater values recorded after 8 weeks than after 2 weeks. In addition, in the late phase of healing, the force magnitude did not have any significant impact on BIC, although it tended to increase with rising forces (0.5 N > 1.0 N > 1.5 N).

Discussion

Recent studies revealed that orthodontic implants can migrate within bone when subjected to orthodontic loading. To investigate whether implants can migrate within bone, *in vivo* micro-CT analyses are a useful tool as multiple high-resolution scans can be obtained from the same animal. Registration of volumetric images from the same animal taken at different time points allows investigating the movement patterns of the implants and the related changes in bone microstructure. Recently, the authors performed a longitudinal *in vivo*

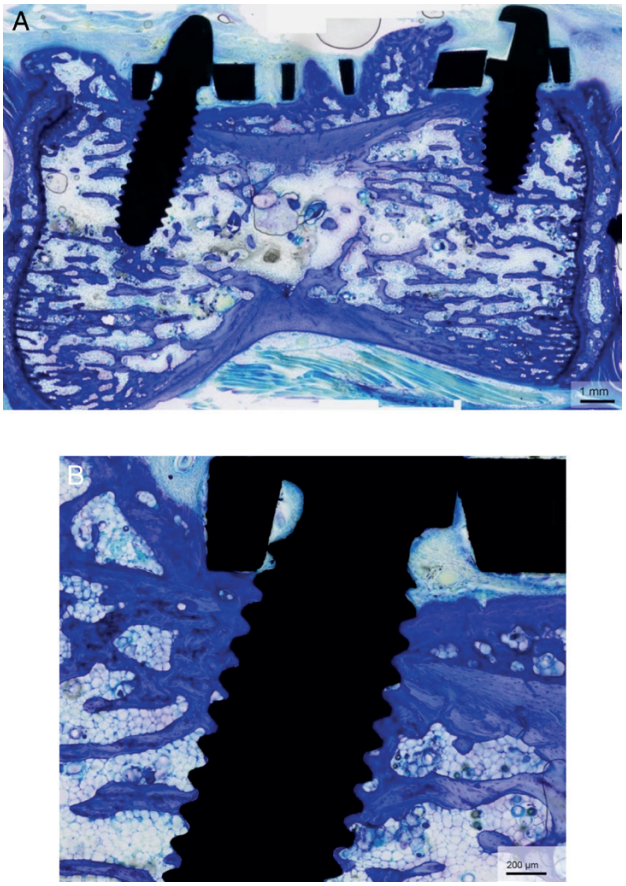

Figure 9. Representative undecalcified histology after 8 weeks of loading (1.0 N) staining with toluidine blue at (a) low and (b) high magnification.

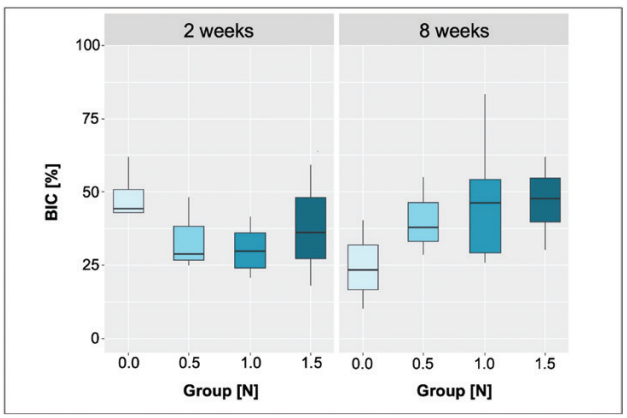

Figure 10. Analysis of the bone-to-implant contact (BIC) at 2 and 8 weeks.

micro-CT study in the rat-tail model and loaded two customized mini-implants per animal by means of flat nickel–titanium spring applying constant forces of 0.0 (control), 0.5, 1.0, and 1.5 N for either 2 or 8 weeks (6). A significant association between implant tip displacement and loading magnitude, as well as significant decrease in migration velocity over time, was observed. Additionally, implant migration was accompanied by bone thickening, especially in the direction of load. The authors suspected that this bone thickening limited implant migration in the late phases of the experiment. Interestingly, characteristic movements of the implants were seen with respect to the different force magnitudes. In the 0.5 N group, movement was almost restricted to the tip, whereas in higher force groups, movements were also noted in the cortical compartment as the centre of resistance shifted downwards.

Although it was demonstrated that implants did not remain stationary stable, a major limitation of micro-CT is that it does not enable investigation of the underlying biological mechanisms. Due to the non-destructive nature of micro-CT, complementary analyses including histology and gene-expression analyses can be performed after sacrificing the animals. Therefore, the present study aimed at providing complementary information at a molecular and cellular level by means of gene and protein expression analyses as well as histomorphometry.

Based on the previous micro-CT data, it was hypothesized that resorption in areas of pressure facilitated implant displacement and that the simultaneous thickening of the bone in the direction of loading further limited implant displacement. Moreover, bone apposition at the original implant position in the 'tension' zones seemed to occur. To validate these hypotheses, additional molecular and histological techniques were required.

The present study revealed no significant differences in osteocytic gene expression with respect to the applied force magnitudes and cell harvesting localization. The difference in relative gene expression of Runx2, sclerostin, and cathepsin K between 'pressure' and 'tension' sites was found to be inverted in the 1.5 N group compared to the remaining groups. Indeed, when high forces were applied (1.5 N), sclerostin levels were higher at the 'tension' compared to the 'pressure' site at 8 weeks of loading, which is in accordance with previous findings reporting decrease of sclerostin levels in the presence of loading (24–27). By contrast, cathepsin K was in general expressed to a higher extent in regions of 'pressure', as also found in previous investigations where it was released from osteocytes in case of mechanical compression (28, 29). The expression of osterix, which is known to be an essential transcription factor for bone formation and mineralization (30, 31), was more pronounced at 2 compared to 8 weeks of loading, with slightly higher values at the 'tension' sites at two weeks of loading. In contrast, at eight weeks, expression was in general more pronounced in the 'pressure' sites. This finding underlines the ongoing bone formation at the original implant positions, which mainly occurred in the early loading phase and the formation of new bone in loading direction limiting bone formation in the later healing phase. Overall, the present data indicated that the local stresses had an impact on the local gene expression, which is in agreement with previous finite element studies on the predicted effects of orthodontic mini-implants on the surrounding bone tissue (32, 33). Although solid scientific data do exist on the role of Runx2 and osterix expression in pre-osteobalsts and osteoblasts (34, 35), there is scarce information on their role in osteocytes. This might be owed to the difficulties encountered so far for the collection of primary osteocyte cultures from mineralized tissue (36). However, studies in mice indicated that Runx2 and osterix regulate osteocytic sclerostin expression through interaction with the promotor of the SOST gene (37, 38).

Analysis of the decalcified histological HE samples revealed an ongoing highly dynamic bone remodelling at 2 weeks of loading in all groups, with a comparable bone architecture in the 'pressure' and 'tension' zones. Only in the 1.5 N group, a pronounced bone thickening accompanied by a reduction of bone marrow spaces was observed in the lateral top ('tension') site. By contrast, numerous mesenchymal stem cells, osteoclasts, and osteoblasts were observed in the lateral bottom ('pressure') site, testifying a different response

of the bone to the higher loading. In this region, the high number of small vessels was likely to be related to intense angiogenesis.

The 0.0 and 0.5 N groups exhibited a similar bone microstructure at 8 weeks of loading. In the 1.0 and 1.5 N groups, newly formed bone presented a characteristic load bearing architecture with trabecula oriented in the direction of the loading. This is in line with a mathematical model simulating the effect of uniaxial bone loading, showing that bone trabeculae were oriented along the direction of loading and in increasing diameter (39). Similar results were also reported in a previous study combining *in vivo* micro-CT and finite elements investigations (40).

The presence of bone remodelling in the cortical compartment in the 1.5 N group at the lateral top ('tension') site might be related to the high level of sclerostin, suggesting a still ongoing implant displacement also confirmed by the *in vivo* micro-CT data.

At 2 weeks, within a distance of 100–200 µm around the implant surface, only a few viable osteocytes were detected in the HE stained samples of the 1.0 and 1.5 N groups. Therefore, special attention was dedicated to cortical bone area inspection as very few osteocytes could be harvested in this region for single cell gene-expression analysis. At high magnification, several lacunae seemed to be empty in this region, which might be related to apoptosis (41), which is also known to induce osteoclastogenesis (42). It would be interesting to further investigate this aspect, such as by means of a terminal deoxynucleotidyl transferase dUTP nick end labeling staining, to better understand viability of osteocytes in the peri-implant tissue (43) and to identify additional extended compartments for cell harvesting in future experiments.

In the present analysis, histomorphometric analyses revealed no significant differences regarding the ratio of EL/TL as well as the BA/TA at both time points of loading, regardless of the localization ('pressure'/'tension') and the applied force. Nonetheless, at 8 weeks of loading, in the test groups (i.e. 0.5, 1, and 1.5 N) higher EL/TL values were registered in areas of 'pressure', and on both 'pressure' and 'tension' sites the values tended to increase with increasing force magnitude. Whether this is related to dying osteocytes in 'pressure' zones, as reported previously (41), has to be studied in future investigations.

Interestingly, one study correlating finite elements investigations for continuously loaded implants with the biological response in the mice model demonstrated wider calcified distance in the area with highest strain intensity (14). They therefore suggested that bone formation activity, particularly the calcification ability of osteoblasts, was locally activated in the highest strain area, which was also reflected in the present histological analysis.

Immunofluorescence analysis confirmed a highly dynamic bone remodelling in the early phase of healing, reflected by the high expression of osteocalcin and cathepsin K at 2 weeks of loading, whereas at 8 weeks their values were almost undetectable. This highlights the almost stable state achieved after 8 weeks of loading.

Undecalcified histology demonstrated bone formation around the implants up to the neck, which is in line with the previous clinical observations reporting stability of migrating implants. Interestingly, the BIC values raised over time and with increasing applied loads. At the time being, there is scarce information on the impact of loading magnitude on BIC values at orthodontic miniscrews. However, it has been demonstrated that early loading did not compromise BIC values at palatal implants, which, however, exhibit rough surfaces (44, 45). Nevertheless, the present data demonstrate that implant migration is not a consequence of bone loss, as suggested previously (46).

Limitations of the present study are related to the limited number of animals available for the respective evaluations. This was due to the fact that the sample size calculation was based on the *in vivo* micro-CT analysis, which had been previously published (6). The aim of the present study was to utilize samples from the previous non-destructive method to enable further investigation of the underlying bone remodelling process at molecular and cell levels. Another limitation is related to the fact that only few genes were examined in the present study, deriving from cells harvested from the cortical compartment in proximity to the implant surface. Histology showed the presence of a limited number of osteocytes up to 300 µm away from the implants, while other cells such as osteoblast-like cells and osteoclasts were populating the areas adjacent to the implants. Therefore, in future studies the authors suggest extending the collection area and including additional types of cells. As bone remodelling is strictly related to angiogenesis (47), also gene-expression assessment of genes involved in new blood vessel formation could be of interest.

The authors are aware that the animal model can affect the remodelling process and migrating level of implants. The rat-tail model was preferred to the rats' jaws, which contain a huge amount of cortical bone tissue, and results would hardly be translatable to humans.

The authors are aware that splitting the peri-implant areas into 'tension' and 'pressure' zones is a simplification and that no conventional 'tension' is possible due to the absence of a periodontal ligament. Indeed, contrary to teeth, the implants are in direct contact with the bone, and forces are directly transmitted to the bone tissue without the interposition of the periodontal ligament.

Additionally, a more accurate assessment of the local stresses and strains would incorporate 3D-micro-finite element models. However, this technique is not applicable to histology, and mapping of non-decalcified histology into the micro-CT volumes is challenging. Nonetheless, the present subdivisions into sectors are in line with the patterns seen with the *in vivo* micro-CT (6). Hence, the simplification of 'pressure' and 'tension' zones, whose definition is familiar to orthodontists, has been adopted.

Finally, another limitation of the study design was the fact that all implants were subjected to immediate loading and that only implants with machined surface were investigated. Hence, future studies might also investigate the impact of different loading time points and surface micro-structures on implant migration at histological and molecular levels (48–50).

Future analyses may include the correlation of micro-CT data with data obtained with emerging technologies like optical coherence tomography, which allows to study the complex three-dimensional cell dynamics in real time.

In conclusion, and within the limitations of the study including lack of statistical significance, the present study underlined that implant migration is associated with extensive bone remodelling in the early loading phase. At this time point, most of the investigated genes were expressed, and also immunoflourescence confirmed expression of proteins related to bone remodelling, i.e. osteocalcin and cathepsin K. Histology revealed marked zones of dynamic bone remodelling with the presence of mesenchymal stem cells, osteoclasts, and osteoblast-like cells. In contrast, at 8 weeks, the bone trabeculae were oriented in the direction of load. At this time point, only in the highest loading group the osteocytic sclerostin levels were reduced at the 'pressure' compared to the 'tension' site, potentially indicating ongoing implant migration. The BIC values increased with respect to the applied force magnitude and timing, thus confirming stable state of the migrating implants.

Supplementary material

Supplementary data are available at *European Journal of Orthodontics* online.

Funding

The study was supported by the Deutsche Forschungsgemeinschaft (DFG, Bonn, Germany, project number: 318755096, reference number: BE 5350/1-1). The Operetta microscope was funded by the Deutsche Forschungsgemeinschaft (INST 208/760-1FUGG to M.B.).

Acknowledgements

The authors would like to thank Dr Alberto Perez Bouza and Simone Enders from the Institute for Pathology and Cytology in Troisdorf, Germany, for the kind support in the preparation of the decalcified sections. The authors would also like to thank the technical assistants Tina Hagena and Brigitte Hartig for the preparation of the undecalcified sections. For the support in the utilization of the laser capture micro-dissection microscope, our thanks go to Dr Stephanie Weidtkamp-Peters and Dr Sebastian Hänsch from the Center for Advanced Imaging (CAi), University of Dusseldorf. Finally, the authors would like to thank Dr Andreas Nagy, Department of Oral Surgery, University Hospital Dusseldorf, for performing the bone-to-implant contact measurements.

Conflicts of interest

None to declare.

Data availability

The data underlying this article will be shared on reasonable request to the corresponding author.

References

1. Liou, E.J., Pai, B.C. and Lin, J.C. (2004) Do miniscrews remain stationary under orthodontic forces? *American Journal of Orthodontics and Dentofacial Orthopedics*, 126, 42–47.
2. Nienkemper, M., Wilmes, B., Pauls, A. and Drescher, D. (2014) Miniimplant stability at the initial healing period: a clinical pilot study. *The Angle Orthodontist*, 84, 127–133.
3. El-Beialy, A.R., Abou-El-Ezz, A.M., Attia, K.H., El-Bialy, A.M. and Mostafa, Y.A. (2009) Loss of anchorage of miniscrews: a 3-dimensional assessment. *American Journal of Orthodontics and Dentofacial Orthopedics*, 136, 700–707.
4. Alves, M., Jr, Baratieri, C. and Nojima, L.I. (2011) Assessment of miniimplant displacement using cone beam computed tomography. *Clinical Oral Implants Research*, 22, 1151–1156.
5. Pittman, J.W., Navalgund, A., Byun, S.H., Huang, H., Kim, A.H. and Kim, D.G. (2014) Primary migration of a mini-implant under a functional orthodontic loading. *Clinical Oral Investigations*, 18, 721–728.
6. Becker, K., Schwarz, F., Rauch, N.J., Khalaph, S., Mihatovic, I. and Drescher, D. (2019) Can implants move in bone? A longitudinal in vivo micro-CT analysis of implants under constant forces in rat vertebrae. *Clinical Oral Implants Research*, 30, 1179–1189.
7. Thalji, G. and Cooper, L.F. (2013) Molecular assessment of osseointegration in vivo: a review of the current literature. *The International Journal of Oral & Maxillofacial Implants*, 28, e521–e534.
8. Becker, K., Stauber, M., Schwarz, F. and Beißbarth, T. (2015) Automated 3D-2D registration of X-ray microcomputed tomography with histological sections for dental implants in bone using chamfer matching and simulated annealing. *Computerized Medical Imaging and Graphics*, 44, 62–68.
9. Becker, K., Schwarz, F., Drescher, D. and Sager, M. (2018) Tierstudien und deren Aussagen. *Implantologie*, 26, 85–91.
10. Stadelmann, V.A., Conway, C.M. and Boyd, S.K. (2013) In vivo monitoring of bone-implant bond strength by microCT and finite element modelling. *Computer Methods in Biomechanics and Biomedical Engineering*, 16, 993–1001.
11. Scheuren, A.C., Vallaster, P., Kuhn, G.A., Paul, G.R., Malhotra, A., Kameo, Y. and Müller, R. (2020) Mechano-regulation of trabecular bone adaptation is controlled by the local in vivo environment and logarithmically dependent on loading frequency. *Frontiers in Bioengineering and Biotechnology*, 8, 566346.
12. Paul, G.R., Malhotra, A. and Müller, R. (2018) Mechanical stimuli in the local in vivo environment in bone: computational approaches linking organ-scale loads to cellular signals. *Current Osteoporosis Reports*, 16, 395–403.
13. Uto, Y., Kuroshima, S., Nakano, T., Ishimoto, T., Inaba, N., Uchida, Y. and Sawase, T. (2017) Effects of mechanical repetitive load on bone quality around implants in rat maxillae. *PLoS One*, 12, e0189893.
14. Okawara, H., Arai, Y., Matsuno, H., Marcián, P., Borák, L., Aoki, K. and Wakabayashi, N. (2021) Effect of load-induced local mechanical strain on peri-implant bone cell activity related to bone resorption and formation in mice: an analysis of histology and strain distributions. *Journal of the Mechanical Behavior of Biomedical Materials*, 116, 104370.
15. Riquelme, M.A., Cardenas, E.R., Xu, H. and Jiang, J.X. (2020) The role of connexin channels in the response of mechanical loading and unloading of bone. *International Journal of Molecular Sciences*, 21, 1146.
16. Bellido, T. (2014) Osteocyte-driven bone remodeling. *Calcified Tissue International*, 94, 25–34.
17. Jilka, R.L., Noble, B. and Weinstein, R.S. (2013) Osteocyte apoptosis. *Bone*, 54, 264–271.
18. Kawamoto, T. and Kawamoto, K. (2014) Preparation of thin frozen sections from nonfixed and undecalcified hard tissues using Kawamot's film method (2012). *Methods in Molecular Biology*, 1130, 149–164.
19. Kilkenny, C., Browne, W., Cuthill, I.C., Emerson, M. and Altman, D.G.; NC3Rs Reporting Guidelines Working Group (2010) Animal research: reporting in vivo experiments: the ARRIVE guidelines. *British Journal of Pharmacology*, 160, 1577–1579.
20. Vandesompele, J., De Preter, K., Pattyn, F., Poppe, B., Van Roy, N., De Paepe, A. and Speleman, F. (2002) Accurate normalization of real-time quantitative RT-PCR data by geometric averaging of multiple internal control genes. *Genome Biology*, 3, RESEARCH0034.
21. Schindelin, J., et al. (2012) Fiji: an open-source platform for biological-image analysis. *Nature Methods*, 9, 676–682.
22. R Core Team (2018) *R, A Language and Environment for Statistical Computing*. R Foundation for Statistical Computing, Vienna, Austria.
23. Bates, D., Mächler, M., Bolker, B. and Walker, S. (2015) Fitting linear mixed-effects models using lme4. *Journal of Statistical Software*, 67, 1–48.
24. Robling, A.G., et al. (2008) Mechanical stimulation of bone in vivo reduces osteocyte expression of Sost/sclerostin. *The Journal of Biological Chemistry*, 283, 5866–5875.
25. Bullock, W.A., Pavalko, F.M. and Robling, A.G. (2019) Osteocytes and mechanical loading: the Wnt connection. *Orthodontics & Craniofacial Research*, 22(Suppl 1), 175–179.
26. Lin, C., Jiang, X., Dai, Z., Guo, X., Weng, T., Wang, J., Li, Y., Feng, G., Gao, X. and He, L. (2009) Sclerostin mediates bone response to mechanical unloading through antagonizing Wnt/beta-catenin signaling. *Journal of Bone and Mineral Research*, 24, 1651–1661.
27. Spatz, J.M., et al. (2015) The Wnt inhibitor sclerostin is up-regulated by mechanical unloading in osteocytes in vitro. *The Journal of Biological Chemistry*, 290, 16744–16758.
28. Dai, R., Wu, Z., Chu, H.Y., Lu, J., Lyu, A., Liu, J. and Zhang, G. (2020) Cathepsin K: the action in and beyond bone. *Frontiers in Cell and Developmental Biology*, 8, 433.
29. Bonnet, N., Brun, J., Rousseau, J.C., Duong, L.T. and Ferrari, S.L. (2017) Cathepsin K controls cortical bone formation by degrading periostin. *Journal of Bone and Mineral Research*, 32, 1432–1441.
30. Liu, Q., Li, M., Wang, S., Xiao, Z., Xiong, Y. and Wang, G. (2020) Recent advances of osterix transcription factor in osteoblast differentiation and bone formation. *Frontiers in Cell and Developmental Biology*, 8, 601224.

31. Nakashima, K., Zhou, X., Kunkel, G., Zhang, Z., Deng, J.M., Behringer, R.R. and de Crombrugghe, B. (2002) The novel zinc finger-containing transcription factor osterix is required for osteoblast differentiation and bone formation. *Cell*, 108, 17–29.
32. Albogha, M.H., Kitahara, T., Todo, M., Hyakutake, H. and Takahashi, I. (2016) Maximum principal strain as a criterion for prediction of orthodontic mini-implants failure in subject-specific finite element models. *The Angle Orthodontist*, 86, 24–31.
33. Stahl, E., Keilig, L., Abdelgader, I., Jäger, A. and Bourauel, C. (2009) Numerical analyses of biomechanical behavior of various orthodontic anchorage implants. *Journal of Orofacial Orthopedics*, 70, 115–127.
34. Hojo, H. and Ohba, S. (2020) Gene regulatory landscape in osteoblast differentiation. *Bone*, 137, 115458.
35. Komori, T. (2020) Molecular mechanism of Runx2-dependent bone development. *Molecules and Cells*, 43, 168–175.
36. Pérez-Campo, F.M., Santurtún, A., García-Ibarbia, C., Pascual, M.A., Valero, C., Garcés, C., Sañudo, C., Zarrabeitia, M.T. and Riancho, J.A. (2016) Osterix and RUNX2 are transcriptional regulators of sclerostin in human bone. *Calcified Tissue International*, 99, 302–309.
37. Sevetson, B., Taylor, S. and Pan, Y. (2004) Cbfa1/RUNX2 directs specific expression of the sclerosteosis gene (SOST). *The Journal of Biological Chemistry*, 279, 13849–13858.
38. Yang, F., Tang, W., So, S., de Crombrugghe, B. and Zhang, C. (2010) Sclerostin is a direct target of osteoblast-specific transcription factor osterix. *Biochemical and Biophysical Research Communications*, 400, 684–688.
39. Kameo, Y., Adachi, T. and Hojo, M. (2011) Effects of loading frequency on the functional adaptation of trabeculae predicted by bone remodeling simulation. *Journal of the Mechanical Behavior of Biomedical Materials*, 4, 900–908.
40. Christen, P., van Rietbergen, B., Lambers, F.M., Müller, R. and Ito, K. (2012) Bone morphology allows estimation of loading history in a murine model of bone adaptation. *Biomechanics and Modeling in Mechanobiology*, 11, 483–492.
41. Noble, B.S., Stevens, H., Loveridge, N. and Reeve, J. (1997) Identification of apoptotic changes in osteocytes in normal and pathological human bone. *Bone*, 20, 273–282.
42. Kogianni, G., Mann, V. and Noble, B.S. (2008) Apoptotic bodies convey activity capable of initiating osteoclastogenesis and localized bone destruction. *Journal of Bone and Mineral Research*, 23, 915–927.
43. Mann, V. and Noble, B. (2019) Techniques for the study of apoptosis in bone. *Methods in Molecular Biology*, 1914, 451–465.
44. Göllner, P., Jung, B.A., Kunkel, M., Liechti, T. and Wehrbein, H. (2009) Immediate vs. conventional loading of palatal implants in humans. *Clinical Oral Implants Research*, 20, 833–837.
45. Jung, B.A., Harzer, W., Wehrbein, H., Gedrange, T., Hopfenmüller, W., Lüdicke, G., Moergel, M., Diedrich, P. and Kunkel, M. (2011) Immediate versus conventional loading of palatal implants in humans: a first report of a multicenter RCT. *Clinical Oral Investigations*, 15, 495–502.
46. Wehrbein, H. and Göllner, P. (2009) Do palatal implants remain positionally stable under orthodontic load? A clinical radiologic study. *American Journal of Orthodontics and Dentofacial Orthopedics*, 136, 695–699.
47. Liu, W.C., Chen, S., Zheng, L. and Qin, L. (2017) Angiogenesis assays for the evaluation of angiogenic properties of orthopaedic biomaterials—a general review. *Advanced Healthcare Materials*, 6. PMID: 28135051. doi:10.1002/adhm.201600434.
48. Freire, J.N., Silva, N.R., Gil, J.N., Magini, R.S. and Coelho, P.G. (2007) Histomorphologic and histomophometric evaluation of immediately and early loaded mini-implants for orthodontic anchorage. *American Journal of Orthodontics and Dentofacial Orthopedics*, 131, 704.e1–e9.
49. Garg, K.K. and Gupta, M. (2015) Assessment of stability of orthodontic mini-implants under orthodontic loading: a computed tomography study. *Indian Journal of Dental Research*, 26, 237–243.
50. Serra, G., Morais, L.S., Elias, C.N., Meyers, M.A., Andrade, L., Müller, C.A. and Müller, M. (2010) Sequential bone healing of immediately loaded mini-implants: histomorphometric and fluorescence analysis. *American Journal of Orthodontics and Dentofacial Orthopedics*, 137, 80–90.